OMAE2019-95767

IMPLEMENTATION OF TIDAL STREAM TURBINES AND TIDAL BARRAGE STRUCTURES IN DG-SWEM

Andrea M. Schnabl [1], Tulio Marcondes Moreira
Engineering Science
University of Oxford
Oxford, OX1 3PJ
United Kingdom

Dylan Wood, Ethan J. Kubatko
Civil, Environmental and Geodetic Engineering
The Ohio State University
Columbus
Ohio, USA

Guy T. Houlsby, Ross A. McAdam, Thomas A.A. Adcock
Engineering Science
University of Oxford
Oxford, OX1 3PJ
United Kingdom

ABSTRACT

There are two approaches to extracting power from tides – either turbines are placed in areas of strong flows or turbines are placed in barrages enabling the two sides of the barrage to be closed off and a head to build up across the barrage. Both of these energy extraction approaches will have a significant back effect on the flow, and it is vital that this is correctly modelled in any numerical simulation of tidal hydrodynamics. This paper presents the inclusion of both tidal stream turbines and tidal barrages in the depth-averaged shallow water equation model DG-SWEM. We represent the head loss due to tidal stream turbines as a line discontinuity – thus we consider the turbines, and the energy lost in local wake-mixing behind the turbines, to be a sub-grid scale processes. Our code allows the inclusion of turbine power and thrust coefficients which are dependent on Froude number, turbine blockage, and velocity, but can be obtained from analytical or numerical models as well as experimental data. The barrage model modifies the existing culvert model within the code, replacing the original cross-barrier pipe equations. At the location of this boundary, velocities through sluice gates are calculated according to the orifice equation. For simulating the turbines, a Hill Chart for low head bulb turbines provided by Andritz Hydro is used.

We demonstrate the implementations on both idealised geometries where it is straightforward to compare against other models and numerical simulations of real candidate sites for tidal energy in Malaysia and the Bristol Channel.

INTRODUCTION

Tidal energy is a promising source of clean and predictable energy. To extract power from the tide the flow needs to pass through a turbine. This can either be a tidal stream turbine or a turbine in a barrage where the flow may be restrained to allow a head to build up. In the latter case it is obvious that there is a substantial interaction between energy extraction and the tidal hydrodynamics but even in the former case it is necessary to apply a force to the flow in order to generate power. Understanding

---

[1]Corresponding author: andrea.schnabl@balliol.ox.ac.uk

these interactions is crucial for evaluating the power output and environmental impact.

To understand these interactions it is necessary to model the basin scale hydrodynamics. Placing tidal turbines or barrages in models at this scale is tricky because of the wide range of length scales involved (see Fig. 5 of [1]). Indeed, there may be some inherent inconsistency, since the flow through turbines is highly three-dimensional and this makes it difficult to conserve mass, momentum and energy fluxes correctly in a 2D or 3D model with a small number of sigma layers.

In this paper we examine the inclusion of both tidal turbines and tidal barrages in DG-SWEM [2, 3]. This numerical model solves the shallow water equations which are generally used for modelling tidal hydrodynamics. The model is based on ADCIRC (ADvanced CIRCulation model) and solves the equations using a discontinuous Galerkin solver [4].

The first half of this paper presents the implementation of tidal stream turbines and presents a number of test cases. The second half does the same but for tidal barrages.

TIDAL STREAM TURBINES
Methodology

Several approaches exist for implementing tidal stream turbines in large scale numerical models (see for instance [5]). One approach is to use enhanced bed friction to represent the thrust from the turbines. A disadvantage of this approach is that it creates ambiguities in terms of the length-scales of the process and exactly what thrust and energy are lost. An alternative approach was developed by Draper [6] who modelled the energy loss as a line sink within the model. Thus a head difference was introduced across the turbine row to represent the energy lost and thrust applied to the turbines. The model was found to be consistent with laboratory measurements [7]. Whilst this approach does reduce the turbine and the wake mixing to a sub-grid scale process, it has the advantage of making it relatively easy to track where the energy is going and does not require very high mesh resolution in the turbine region. This approach was implemented in the discontinuous Galerkin version of AD-CIRC by Serhadlıoğlu [8]. She used actuator disc theory to represent the turbines following [9]. Her model has been widely used (e.g. [10–12]).

The present work takes the line-discontinuity approach and implements this in DG-SWEM. In contrast to Serhadlıoğlu's turbine implementation, the one discussed in this paper is based on an input of power and thrust coefficient curves, which in turn can be obtained from any external analytical or numerical model as well as from experimental data. This leads to more flexibility in terms of turbine model selection. In this paper two external turbine models have been used: (i) the analytical Linear Momentum Actuator Disc Theory (LMADT) model and (ii) a model based on experimental and numerical data for the cross-flow Transverse
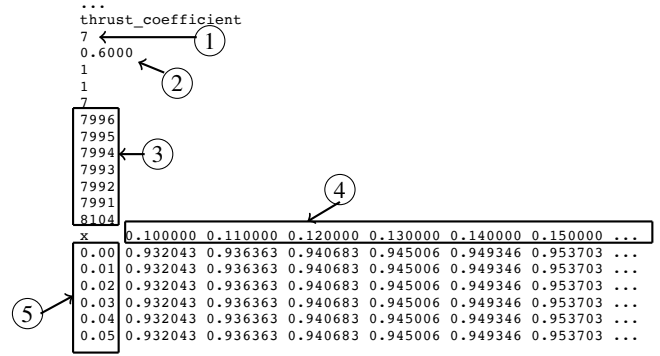

FIGURE 1: C_t-PART OF AN EXAMPLE INPUT FILE

Horizontal Axis Water Turbine (THAWT). The results of the former are compared to Serhadlıoğlu's implementation to ensure correct execution of the input method. Both underlying models are described below, but others could be adopted as well.

To implement the turbine characteristics DG-SWEM's nodal attribute input file (fort.13) was adapted to include tables for thrust coefficient C_t and power coefficient C_p with respect to upstream Froude number $Fr = u/\sqrt{gh}$ and local blockage $B = A_t/(hb)$, where u is flow velocity, h water depth and g gravitational acceleration, and with turbine swept area A_t, and local passage width b. These tables are assigned to turbine nodes. An additional input parameter is the turbine swept area per unit length. In the modified DG-SWEM code used in this paper the actual thrust and power coefficients are interpolated from these tables for edges between consecutive turbine nodes along the specified turbine arrays. These, in turn, are used to calculate the thrust on the flow and the power generation. The energy loss due to local wake-mixing behind the turbines is considered to be a sub-grid scale process. A schematic representation of an example input file table for C_t can be found in Fig. 1. The numbered elements in Fig. 1 represent the following: (1) number of turbine nodes, (2) turbine swept area per unit length, (3) list of turbine nodes, (4) local blockage B, and (5) Froude number Fr. The lines in between (2) and (3) represent, in the following order, a constant to determine if all turbine nodes have the same characteristics, the number of turbine arrays, and the number of turbine nodes in the first array. The table for C_p is constructed similarly and part of the same input file.

Actuator disc model The simplest representation of a tidal turbine in a flow is that given by actuator disc theory. In the present paper we use the formulation given in [6, 9] which forms the basis for the turbine model in [8]. The inputs to the model are upstream flow conditions (i.e. Fr), blockage ratio B, and turbine tuning (i.e. α_4). The model gives the head difference between the upstream and downstream as well as the 'available'

power output – i.e. the power extracted from the flow minus the energy lost in wake mixing behind the turbines. This model is well documented in the literature (e.g. [10, 13]) so we do not describe it in detail here.

THAWT model The second turbine model is based on experimental and numerical data from the Transverse Horizontal Axis Water Turbine (THAWT) [14–16]. The experiments were conducted on a prototype with a turbine diameter of 0.5 m, two different blockage ratios $B = 0.47$ and $B = 0.59$, and various Froude numbers [14]. To account for device scaling, such as Reynolds number effects, Stringer et al. [17] carried out 2D Reynolds-Averaged numerical simulations of the turbine, both at laboratory scale and full scale. The results from both experimental and numerical investigations were then used to find correlations for maximum power and thrust coefficients with respect to Reynolds number Re, Froude number Fr, and blockage ratio B. At $Re < 550000$ and calibrated for a range of blockage ratios between $B = 0.47$ and $B = 0.59$ these correlations are as follows:

$$
\begin{aligned}
C_{p,max} &= 0.952 log(Re/550000) \\
&\quad + (-0.401 + 2.47B) + (4.898 - 6.65B)Fr, \\
C_{t,max} &= 0.619 log(Re/550000) \\
&\quad + (-3.627 + 11.835B) + (18.27 - 29.71B)Fr.
\end{aligned}
\tag{1}
$$

While at $Re > 550000$ the following apply:

$$
\begin{aligned}
C_{p,max} &= 0.197 log(Re/550000) \\
&\quad + (-0.401 + 2.47B) + (4.898 - 6.65B)Fr, \\
C_{t,max} &= 0.152 log(Re/550000) \\
&\quad + (-3.627 + 11.835B) + (18.27 - 29.71B)Fr.
\end{aligned}
\tag{2}
$$

In order to include the effects of varying tip speed ratios λ the experimental data was used to fit curves like the ones shown schematically in Fig. 2.

In this analysis the turbines are assumed to operate at the optimum tip speed ratio λ to give $C_{p,max}$. We do not consider "tuning" of turbines (see [18, 19]).

RESULTS

To test the implementation of the turbine code several test cases of an idealised channel with both steady and unsteady conditions have been evaluated. Furthermore, a more realistic model of the Malacca Strait based on a previous study [12], has been investigated. The results are discussed below.
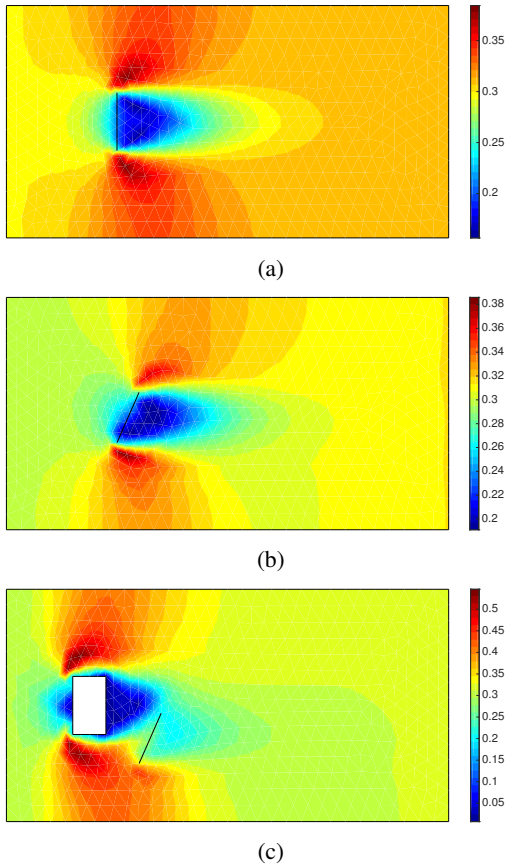
Steady idealised channel The idealised channel is 40 km long and 10 km wide with a water depth of 15 m. The bed
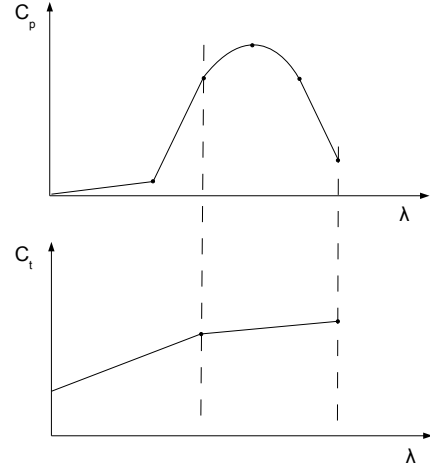
FIGURE 2: SCHEMATIC OF C_p AND C_t CURVES FOR THAWT MODEL

friction is set to $c_f = 0.0005$. The top and bottom boundaries of the channel are tangential slip boundaries and the right boundary is set to a constant elevation of zero. In the steady case the left boundary is forced with a constant flow rate ($Fr \approx 0.1$). Different variations of tidal fences have been investigated: (i) a tidal fence spanning the entire width of the channel; (ii) a tidal fence partially spanning the width of the channel; (iii) the tidal fence from (ii) rotated by an angle of 30 degrees; (iv) the tidal fence from (iii) placed downstream of a rectangular island. All turbine fences have the same characteristics ($\alpha_4 = 1/3$ and $B = 0.5$).

Fig. 3 shows contour plots for three of the steady cases with the C_p and C_t curves derived from the LMADT model. The three plots in Fig. 3 show the depth-averaged velocity magnitude. The acceleration of the bypass flow and the deceleration of the core flow can be seen especially in Fig. 3a. Both Figs. 3b and 3c demonstrate the ability of the code to cope with flow that is not perpendicular to the turbine fence. The different implementations of the actuator disc model (hard-coded or via input file) compare very well, which can be seen in Fig. 4 for both the full tidal fence (Fig. 4a) and the partial tidal fence (Fig. 4b). Here, the 'LMADT' corresponds to the hard-coded version of [8], while the implementation via input file for both LMADT and THAWT models are represented by the 'P-T-curves, LMADT' and 'P-T-curves, THAWT', respectively. The corresponding result for the tidal fence angled to the input flow and the tidal fence downstream of the island are not shown here, but show similar agreement for the two models. The differences in the beginning of the simulation period are a result of different ramp functions. The power achieved with the THAWT model is lower than with the LMADT model for both the full and the partial tidal fence. This is to be expected as the THAWT model is based on experimental data and therefore accounts for losses

(a)

(b)

(c)

FIGURE 3: DEPTH-AVERAGED VELOCITY FOR (a) CASE (ii), (b) CASE (iii), (c) CASE (iv)

that the more idealised LMADT model does not capture.

Unsteady idealised channel   For the unsteady case the channel geometry and meshing remains the same as in the steady case, but the left boundary is now forced with a sinusoidal elevation of amplitude $A = 0.05$ m and period of $T = 12.42$ h. All other boundaries and turbine characteristics remain the same. Fig. 5 again shows the power generation over time for all three models for the full tidal fence (Fig. 5a) and the partial array (Fig. 5b). Again, the agreement between the two LMADT models is very good. Similar to the steady case the power output from the THAWT model is lower than the one from the LMADT model for both the full and partial array. The difference between two consecutive peaks (different directions of flow) can be ascribed to the free surface. A flow direction left-to-right means a slightly higher water depth, compared to a mean water depth of 15 m, at the turbine fence than for the opposite direction. Thus, the flow speed is higher for the direction right-to-left, which in turn leads to a higher power generation.


(a)

(b)
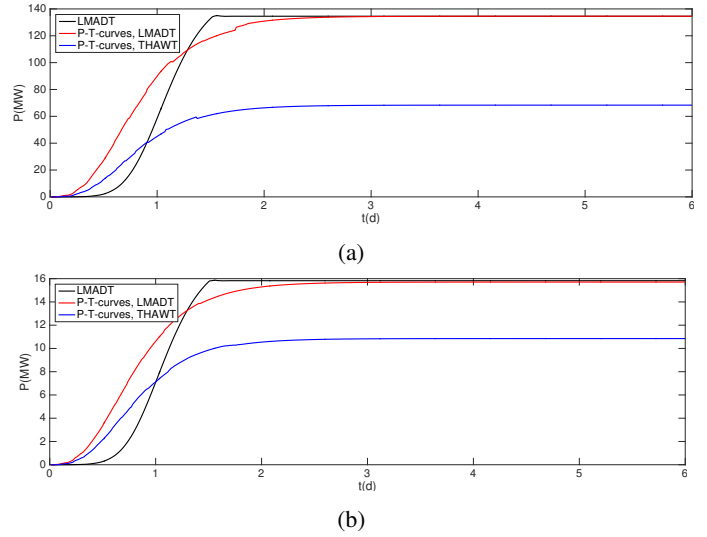
FIGURE 4: COMPARISON OF POWER FOR ALL THREE TURBINE MODELS FOR (a) FULL TURBINE FENCE, (b) PARTIAL TURBINE FENCE – STEADY

(a)

(b)
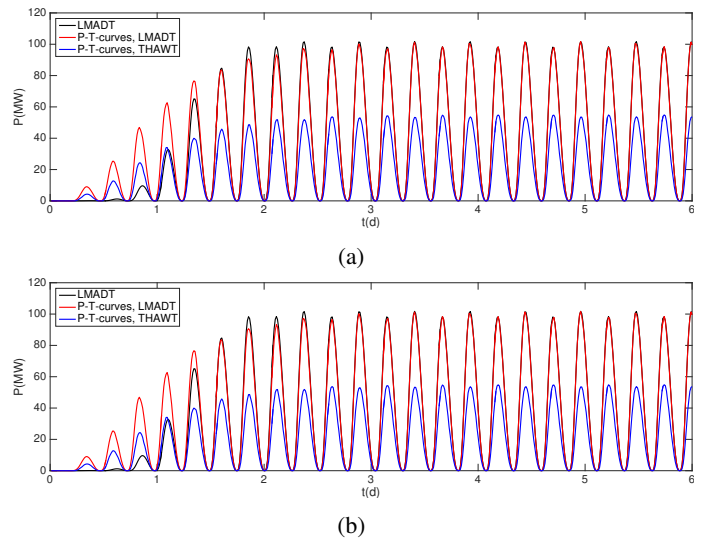
FIGURE 5: COMPARISON OF POWER FOR ALL THREE TURBINE MODELS FOR (a) FULL TURBINE FENCE, (b) PARTIAL TURBINE FENCE – UNSTEADY

The Froude number and blockage ratio intervals for the C_p and C_t tables in the input file (see Fig. 1) can in principle be chosen arbitrarily, but Fig. 6 shows that they require some attention. There, the power generation of one full cycle for three different interval sizes (ΔFr and $\Delta B = 0.01$, 0.05 and 0.1) for the case of the actuator disc model with $B = 0.4$ is plotted (Fig. 6). While the results for the 0.01 and 0.05 cases agree well, the 0.1 case
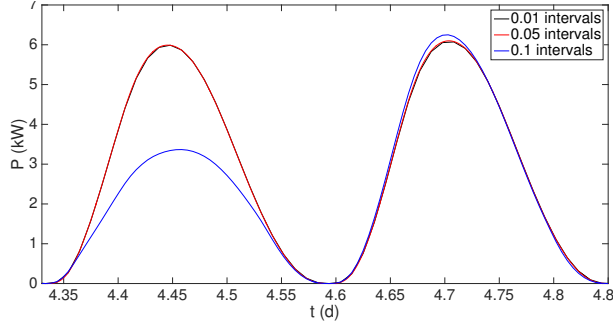
FIGURE 6: COMPARISON OF DIFFERENT INPUT TABLE STEP SIZES FOR THE ACTUATOR DISC MODEL

differs significantly. Therefore, a convergence study should be undertaken to determine the step size.

Malaysia model The model of the Malacca Strait by Bonar et al. [12] is used for the last part of the test. The numerical mesh of the entire domain can be seen in Fig. 7a. The land boundaries are set to allow tangential slip, while the open ocean boundary is forced with tidal constituents and a constant northwest-going flow [12]. Two tidal fences are placed at the Port Dickson location (see Fig. 7b) with a local blockage ratio of $B = 0.5$ and a turbine wake velocity coefficient of $\alpha_4 = 1/3$ for the actuator disc model.

The new implementation of the actuator disc model C_p and C_t curves again compares well to the previous hard-coded implementation, as can be seen in the power output in Fig. 8. The top subplot Fig. 8a shows the differences in the spring-neap cycle, which are captured by all three models. As for the idealised cases, the THAWT model leads to a lower power output than the actuator disc models as it accounts in more detail for realistic hydrodynamic losses. Fig. 8b represents a shorter time interval, which shows that the general form, if not the magnitude, of the power variations is captured by the THAWT model as well.

In addition to the power generation of the turbine arrays, the environmental impact is another factor that needs to be considered. Processes like sediment transport or distribution of nutrients can be significantly effected by changes to the natural flow speed. While this is not a comprehensive environmental study, the change in flow speed can provide some understanding of the potential environmental impact. Fig. 9 shows the change in depth-averaged velocity at peak power for the actuator disc model – the THAWT model gives visually similar results. Both turbine models lead to a significant change in flow velocity. The downstream flow throughout the entire length of the turbine arrays is slowed down due to the energy extraction. The bypass flow around the turbine fences on the other hand is accelerated.

TIDAL BARRAGES AND LAGOONS

In the second section we present the implementation of a tidal barrage boundary in DG-SWEM. For this work we adopted a 'two-way' generation strategy (see [20, 21]) of which the various phases are shown schematically in Fig. 10.

Methods

For including the effects of sluices and turbines inside DG-SWEM, modifications were made to an existing culvert model [22, 23]. The culvert boundary incorporates an internal barrier into the mesh that connects pairs of nodes across the "barrier" segment (Fig. 11). The flow between these pairs is found from the water level difference between "Front" and "Back" sides.

In order to simulate a tidal barrage behaviour, the culvert equations are substituted by appropriate sluice and turbine equations, along with a control switch for starting and ending power generation. For the sluice gates, the orifice equation has been extensively used in the literature as an appropriate representation of flow through hydraulic structures [20, 24]

$$Q_o(H) = C_d A_S \sqrt{2gH}, \tag{3}$$

where C_d is the discharge coefficient (chosen as "1" for this study), A_S the sluice area, g the gravity constant and H the head difference between the ocean and the impounded body of water.

To obtain the flow through the turbines and power characteristics a Hill Chart is used. In the current work we use a low head bulb turbine Hill Chart provided by Andritz Hydro [25, 26]. This chart relates the turbine unit speed n_{11} with the specific unit discharge Q_{11} obtained experimentally. The graph also shows the efficiency curves η, wicked gate openings and pitch blade opening.

By specifying the turbine diameter D, number of generating poles G_p and grid frequency f, the turbine rotation S_p (rpm) is obtained as $S_p = \frac{120f}{G_p}$ where the unit speed n_{11} and specific discharge Q_{11} are:
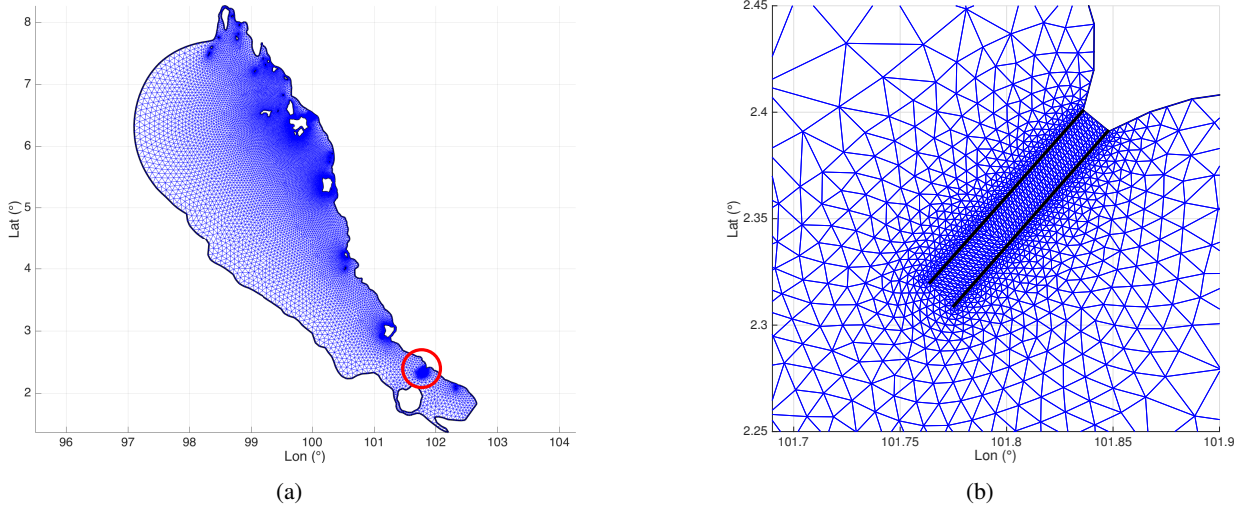
$$n_{11} = \frac{S_p D}{\sqrt{H}}, \quad Q_{11} = \frac{Q_t}{D^2 \sqrt{H}}. \tag{4}$$

Manipulating Eqn. (4), the head difference H can be described as

$$H = \left(\frac{S_p D}{n_{11}}\right)^2. \tag{5}$$

In turn, the turbine flow-rate Q_t can be obtained from Eqn. (4):

$$Q_t = Q_{11} D^2 \sqrt{H}, \tag{6}$$

5

FIGURE 7: NUMERICAL MESH OF (a) THE WHOLE DOMAIN, (b) THE TURBINE AREA AROUND PORT DICKSON

so that power output P is

$$P = |\rho g Q_t H \eta|, \tag{7}$$

where ρ is the water density. With the presence of a forcing head, n_{11} is obtained from Eqn. (4), while Q_{11} can be attained from regulating the (i) opening of the wicked gate, (ii) pitching of the runner blade and crossing the values with the obtained n_{11}. The maximum output plot is obtained by digitizing the chart [25], and following the path where the product between η, Q and H is maximized. Yielding the functions:

$$
\begin{aligned}
Q_{11} &= (0.0166)n_{11} + 0.4861; \; (\text{when } n_{11} =< 255) \\
Q_{11} &= 4.75; \; (\text{when } n_{11} > 255)
\end{aligned}
\tag{8}
$$

and,

$$\eta = (-0.0019)n_{11} + 1.2461. \tag{9}$$

Knowing the head difference yields n_{11}, both flow-rate and power through the turbines can be calculated using Eqn. (6)-(9).

A ramp function of 20 minutes is included to avoid sharp changes between the different stages of barrage operation consistent with that used in other representations of barrages [27, 28].

Idealised model   Considering the implementation in an idealised geometry. We evaluate the rectangular domain shown in Fig. 12 where an internal barrier connects the node pairs between Sections 1 and 2. In the case study shown, 15 node pairs

are selected to simulate sluice gates, each having an area equivalent to a 7m diameter orifice and a single control switch for allowing flow to pass when $H >= 1.5m$. In order to drive the flow through the sluices, a sinusoidal component, with 3m amplitude and 12.42h period is applied to the rectangular domain on the left, while the other domain is set to have a constant water level (Point-1 and 2, Fig. 13). A 0D model, based on the orifice equation, utilises the combined sluice area by the node pairs and the head difference from Fig. 13 to estimate the analytical flow Q_e expected to flow through the boundary. Detailed examination of the flows shows that mass is conserved across the barrier.

The Swansea Lagoon Project

In this section the barrage boundary is used to simulate the Swansea Bay Tidal Lagoon project suggested for the Bristol Channel. We insert the lagoon representation into the numerical model with hydrodynamics developed in [29] and [30]. The mesh of this model is shown in Fig. 14. In this study we only consider forcing from the M_2 tidal constituent.

For simulating the Swansea Lagoon, a number of node pairs are selected according to the lagoon design, so that the positioning of both turbines and sluices are as accurate as possible. At the lagoon site, extra refinement is used in the region where turbines and sluices are installed. In order not to increase the mesh resolution excessively at the location of the hydraulic structures, each node pair was responsible for simulating a number of turbines or sluices. For this case study, we use a set up of 16 turbines with 7.35m in diameter and 95 generating poles each. They operate together with a total sluice area of 800m^2, feeding a grid with frequency $f = 50Hz$.
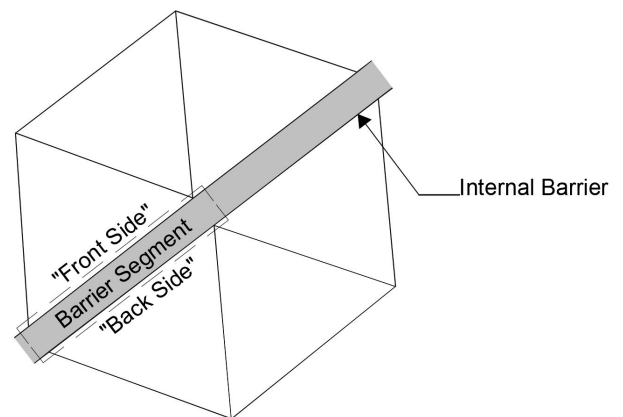
6
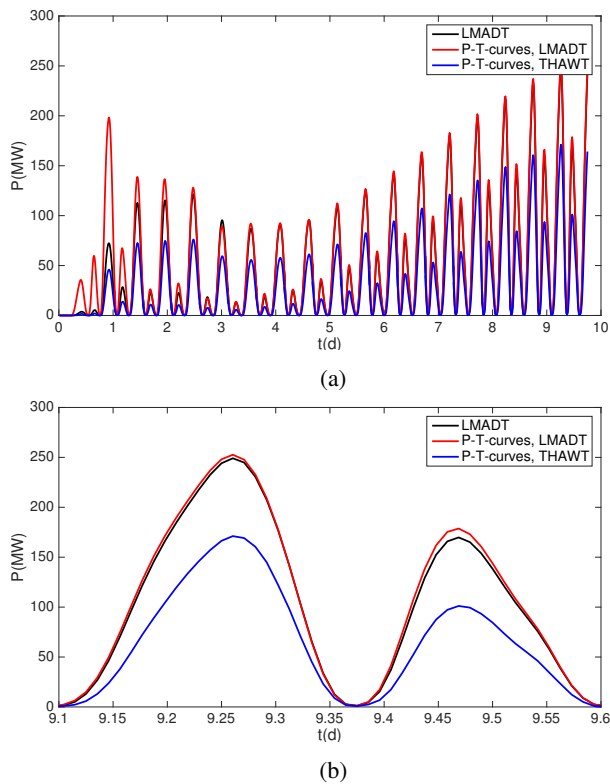
FIGURE 8: COMPARISON OF POWER FOR ALL THREE TURBINE MODELS FOR (a) ENTIRE SIMULATION PERIOD, (b) ONE TIDAL CYCLE
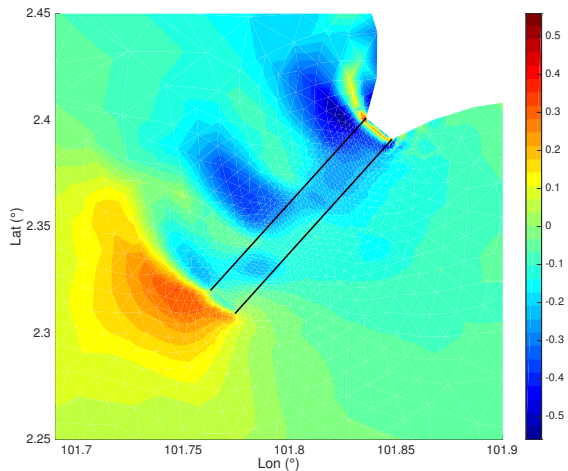
FIGURE 9: CHANGE IN DEPTH-AVERAGED VELOCITY AT PEAK POWER FOR THE LMADT MODEL
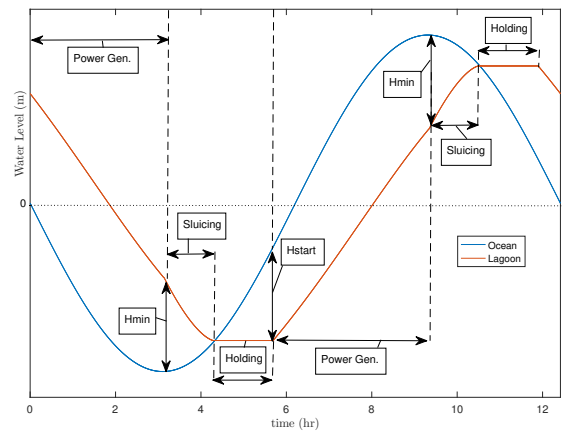
FIGURE 10: REPRESENTATION OF A TWO-WAY SCHEME WITH STARTING (HSTART) AND FINISHING HEADS (HMIN) FOR TURBINE OPERATION FOR A WHOLE CYCLE.


FIGURE 11: INTERNAL BARRIER AND TRIANGULAR ELEMENT REPRESENTATION (AFTER: [23]).

Power Production Verification (0D vs 2D) For verifying power production from the 2D model, a 0D model (following [24]) was used. The 0D model solves for the flow inside the barrage (assuming the water to be level) for a given water elevation outside the barrage. In this study we take the water level from the 2D model outside the barrage as the driver for our 0D model. After fixing the number of sluices, turbines and lagoon size, power extraction becomes highly dependent on the starting $Hstart$ and finishing $Hmin$ operational heads chosen for the simulation (see [31]). We do not consider detailed optimisation here, but consider two cases of different operations, with Case 1 having $Hstart = 2.5m$ and $Hmin = 1.5m$, following a recommended design by [28], and Case 2 with $Hstart = 2.0m$ and
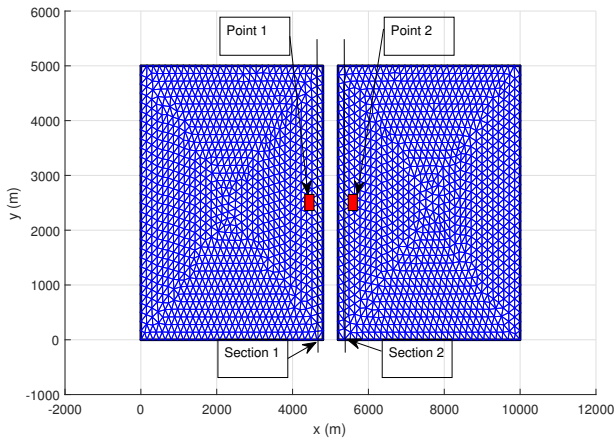
FIGURE 12: RECTANGULAR MODELS USED FOR MASS CONSERVATION CHECK.
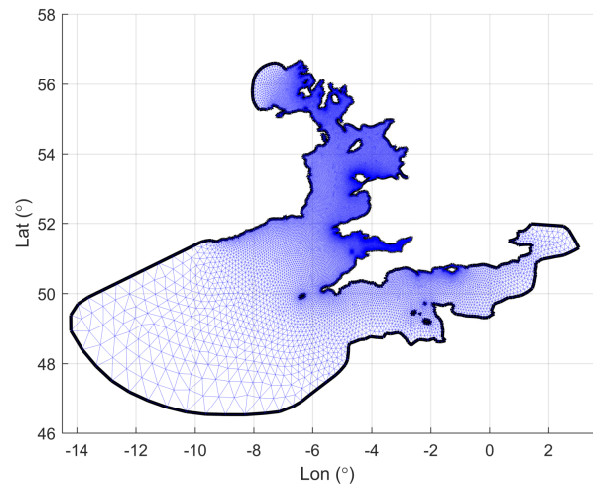
FIGURE 14: COMPLETE 2D MODEL IN ADCIRC.
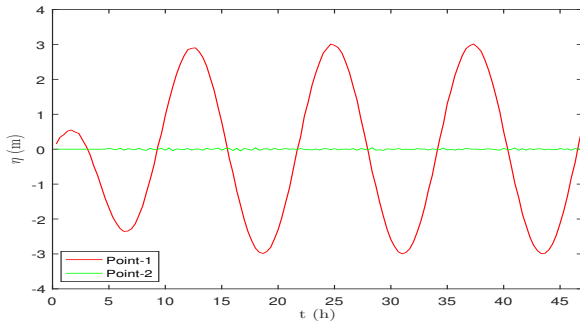
FIGURE 13: WATER LEVEL MOTION OF POINTS 1 AND 2 FROM RECTANGULAR MODEL.

$Hmin = 1.0m$, for comparison.

For a simulation run of 212 hours, 0D and 2D power outputs (P_e and P_n, respectively) from Cases 1 and 2 are plotted against each other (Fig. 15) where the water level from the 0D was taken from the 2D model (thus accounting for the change in tidal amplitude outside the barrage due to the presence of the barrage). 0D and 2D methods show good agreement of results, although there is some deviation observed. The water level inside the lagoon not being exactly flat and small water level variations across the different turbine mean that the agreement is not exact. Integrated over the cycle the difference between the two models is of the order of a few percent.

This paper does not present an in depth analysis of the power output from the Swansea Bay lagoon scheme. However, we note that the mean power predicted by our model (32.69 MW and 25.52 MW for Case 1 and 2 respectively) is consistent with the estimate given by the developers given that we are only consid-

ering a single tidal constituent.

CONCLUSIONS

When conducting large scale modelling of tidal energy schemes it is important to represent the energy extraction from the system in a way which is consistent and physically reasonable. This can be problematic since the local flows around energy extraction systems are too complex to directly model in large scale models. Once the correct physics has been developed it is also important to verify its implementation. The present work focuses on achieving this.

In this paper we have presented implementations of tidal stream turbines and tidal barrages in the shallow water equation code DG-SWEM. We have used idealised models to compare our implementations with other results from either well validated models or simpler models. We find acceptable agreement for all cases. Further, we have implemented both models in numerical simulations of real location which are candidate sites for tidal energy development. Our results from these real sites are in agreement with expectations.
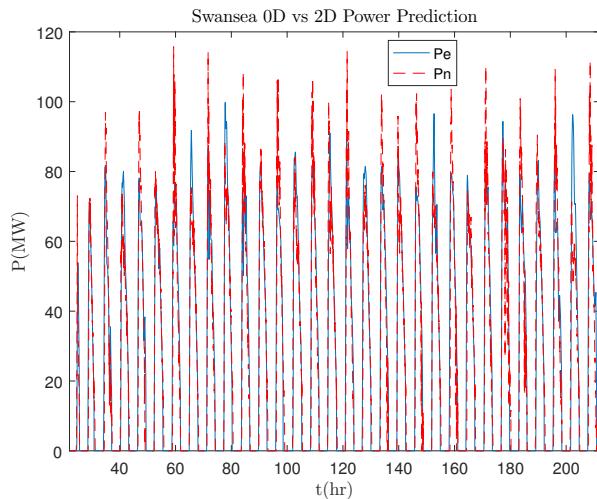
REFERENCES

[1] Adcock, T. A. A., Draper, S., and Nishino, T., 2015. "Tidal power generation–a review of hydrodynamic modelling".
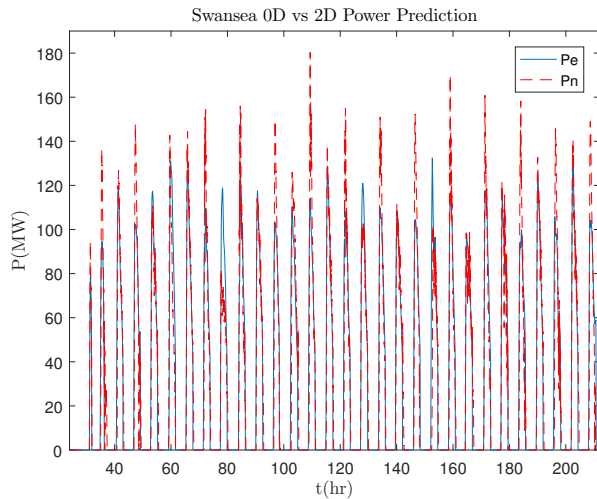
(a) Case 1

(b) Case 2

FIGURE 15: POWER OUTPUT COMPARISON FOR 0D AND 2D CASES (P_e AND P_n, RESPECTIVELY).

    Proc. IMechE A: J. Pow. and Energy, **229**(7), pp. 755–771.

[2] Kubatko, E. J., Westerink, J., and Dawson, C., 2006. "hp Discontinuous Galerkin methods for advection dominated problems in shallow water flow". *Computer Methods in Applied Mechanics and Engineering,* **196**(13), pp. 437–451.

[3] Bunya, S., K. E. W. J., and Dawson, C., 2009. "A wetting and drying treatment for the Runge–Kutta discontinuous Galerkin solution to the shallow water equations". *Computer Methods in Applied Mechanics and Engineering,* **198**(17), pp. 1548–1562.

[4] Kubatko, E. J., Bunya, S., Dawson, C., Westerink, J. J., and Mirabito, C., 2009. "A Performance Comparison of Continuous and Discontinuous Finite Element Shallow Water Models". *Journal of Scientific Computing,* **40**(1), pp. 315–339.

[5] Vogel, C. R., Willden, R. H. J., and Houlsby, G. T., 2013. "A correction for depth-averaged simulations of tidal turbine arrays". In Proceedings of the 10th European Wave and Tidal Energy Conference (EWTEC), Aalborg, Denmark, Vol. 25.

[6] Draper, S., 2011. "Tidal Stream Energy Extraction in Coastal Basins". D.Phil. thesis, University of Oxford.

[7] Draper, S., Stallard, T., Stansby, P., Way, S., and Adcock, T. A. A., 2013. "Laboratory scale experiments and preliminary modelling to investigate basin scale tidal stream energy extraction". In 10th European Wave and Tidal Energy Conference (EWTEC), Aalborg, Denmark.

[8] Serhadlıoğlu, S., 2014. "Tidal stream resource assessment of the Anglesey Skerries and the Bristol Channel". D.Phil. thesis, University of Oxford.

[9] Houlsby, G. T., Draper, S., and Oldfield, M. L. G., 2008. Application of linear momentum actuator disc theory to open channel flow. Tech. Rep. OUEL 2296/08, Department of Engineering Science, University of Oxford.

[10] Adcock, T. A. A., Draper, S., Houlsby, G. T., Borthwick, A. G. L., and Serhadlıoğlu, S., 2013. "The available power from tidal stream turbines in the Pentland Firth". *Proc. R. Soc. A,* **469**(2157), p. 20130072.

[11] Adcock, T. A. A., Draper, S., Houlsby, G. T., Borthwick, A. G. L., and Serhadlıoğlu, S., 2014. "Tidal stream power in the Pentland Firth–long-term variability, multiple constituents and capacity factor". *Proc. IMechE A: J. Pow. and Energy,* **228**(8), pp. 854–861.

[12] Bonar, P. A. J., Schnabl, A. M., Lee, W.-K., and Adcock, T. A. A., 2018. "Assessment of the Malaysian tidal stream energy resource using an upper bound approach". *in press, Journal of Ocean Engineering and Marine Energy*.

[13] Draper, S., Houlsby, G. T., Oldfield, M. L. G., and Borthwick, A. G. L., 2010. "Modelling tidal energy extraction in a depth-averaged coastal domain". *IET Renewable Power Generation,* **4**(6), pp. 545–554.

[14] McAdam, R. A., Houlsby, G. T., and Oldfield, M. L. G., 2013. "Experimental measurements of the hydrodynamic performance and structural loading of the transverse horizontal axis water turbine: Part 1". *Renew. Energy,* **59**, pp. 105 – 114.

[15] McAdam, R. A., Houlsby, G. T., and Oldfield, M. L. G., 2013. "Experimental measurements of the hydrodynamic performance and structural loading of the transverse horizontal axis water turbine: Part 2". *Renew. Energy,* **59**, pp. 141 – 149.

[16] McAdam, R. A., Houlsby, G. T., and Oldfield, M. L. G., 2013. "Experimental measurements of the hydrodynamic

performance and structural loading of the transverse horizontal axis water turbine: Part 3". *Renew. Energy, 59*, pp. 82 – 91.

[17] Stringer, R., Hillis, A., and Zang, J., 2016. "Numerical investigation of laboratory tested cross-flow tidal turbines and Reynolds number scaling". *Renew. Energy, 85*, pp. 1316 – 1327.

[18] Vennell, R., 2010. "Tuning turbines in a tidal channel". *Journal of Fluid Mechanics, 663*, 11, pp. 253–267.

[19] Vennell, R., and Adcock, T. A. A., 2014. "Energy storage inherent in large tidal turbine farms". *Proc. R. Soc. A, 470*(2166).

[20] Baker, A. C., 1991. *Tidal Power*. Institution of Engineering and Technology (1711).

[21] Neill, S. P., Angeloudis, A., Robins, P. E., Walkington, I., Ward, S. L., Masters, I., Lewis, M. J., Piano, M., Avdis, A., Piggott, M. D., Aggidis, G., Evans, P., Adcock, T. A. A., Zidonis, A., Ahmadian, R., and Falconer, R., 2018. "Tidal range energy resource and optimization–past perspectives and future challenges". *Renewable Energy, 127*, pp. 763–778.

[22] Westerink, J.J., L. R., and Militello, A., 2001. Leaky Internal-Barrier Normal-Flow Boundaries in the ADCIRC Coastal Hydrodynamics Code. Chetn, US Army Corps of Engineers, June.

[23] Dawson, C., Kubatko, E. J., Westerink, J. J., Trahan, C., Mirabito, C., Michoski, C., and Panda, N., 2011. "Discontinuous Galerkin methods for modeling Hurricane storm surge". *Adv. Water Resources, 34*(9), pp. 1165 – 1176. New Computational Methods and Software Tools.

[24] Prandle, D., 1984. "Simple theory for designing tidal power schemes". *Advances in water resources, 7*(1), pp. 21–27.

[25] Aggidis, G., and Feather, O., 2012. "Tidal range turbines and generation on the Solway Firth". *Renewable energy, 43*, pp. 9–17.

[26] Aggidis, G., and Benzon, D., 2013. "Operational optimisation of a tidal barrage across the Mersey estuary using 0-D modelling". *Ocean Engineering, 66*, pp. 69–81.

[27] Bray, S., A. R., and Falconer, R., 2016. "Impact of representation of hydraulic structures in modelling a Severn barrage". *Comp. & Geosci., 89*, pp. 96–106.

[28] Angeloudis, A., Falconer, R., Bray, S., and Ahmadian, R., 2016. "Representation and operation of tidal energy impoundments in a coastal hydrodynamic model". *Renewable energy, 99*, pp. 1103–1115.

[29] Serhadlıoğlu, S., Adcock, T. A. A., Houlsby, G. T., Draper, S., and Borthwick, A. G. L., 2013. "Tidal stream energy resource assessment of the Anglesey Skerries". *International Journal of Marine Energy, 3*, pp. e98–e111.

[30] Adcock, T. A. A., and Draper, S., 2014. "On the tidal stream resource of two headland sites in the English Channel: Portland Bill and Isle of Wight". In ASME 2014 33rd International Conference on Ocean, Offshore and Arctic Engineering, American Society of Mechanical Engineers, pp. V09AT09A003–V09AT09A003.

[31] Ahmadian, R., Xue, J., Falconer, R. A., and Hanousek, N., 2017. "Optimization of tidal range schemes". *Proceedings of the 12th European Wave and Tidal Energy Conference 27th Aug-1st Sept 2017, Cork, Ireland.*